JOURNAL OF AIRCRAFT
Vol. 48, No. 3, May–June 2011

Modeling of Wing Rock Using Frequency Spectrum Analysis to Free-to-Roll Time History

Bing Wang,* Xue-Ying Deng,† Bao-Feng Ma,‡ Zhen Rong,§ and Bo-Chao Cao¶
Beijing University of Aeronautics and Astronautics, 100191 Beijing, People's Republic of China

DOI: 10.2514/1.C000201

A systematic method is presented for modeling wing rock of one degree of freedom. This method is based on the frequency spectrum analysis to free-to-roll time history. The frequency analysis reveals that there are other higher-frequency components in the rolling angular acceleration time history of wing rock, with the exception of the main frequency. Among them, the energy at the triple frequency relative to the main frequency is greater than others. The central idea of the method presented for modeling wing rock is the summation of several sine waves for which the frequencies include main frequency, double-main frequency, and triple-main frequency. The structure and parameters of the modeled dynamic equations are all determined by the frequency analysis of the rolling angular acceleration time history of the wing rock. The simulated results based on this model agree well with the experimental data.

Nomenclature

A	=	amplitude of wing rock, °.
b	=	wing span, m
C_l	=	rolling moment coefficient
f	=	frequency of wing rock, Hz
I_{xx}	=	model inertia, kg · m^2
S	=	wing area, m^2
u_∞	=	freestream velocity, m/s
ρ	=	air density, kg/m^3
ϕ	=	roll angle of model, °.
φ	=	phase angle, rad
ω	=	circular frequency of oscillation ($2\pi f$), rad/s
$\dot{}$	=	derivative with respect to time

I. Introduction

MANEUVERABILITY and agility were very important for modern combat aircraft, and the improvement of the maneuverability and agility of the combat aircraft were very dependent on the ability of flight at high angles of attack. When the aircraft was flying at a high angle of attack, some uncontrolled flight phenomena were possibly produced due to the flow deterioration, and wing rock was one of them. The wing rock was characterized by a self-induced limit-cycle oscillatory motion in roll. The occurrence of the wing rock would impact the stability and control of the aircraft and bring a lot of problems to flight security. As a result, great attention had been paid to it by lots of researchers [1,2].

To model the wing rock phenomenon, some researchers [3–9] had tried to give some dynamic equations to model the motions of wing rock. In these modeled dynamic equations, the coefficients need be measured in wind-tunnel tests or be calculated using computational fluid dynamics techniques.

In this paper, a novel method for modeling wing rock of one degree of freedom was presented, and it was only based on the data of free-to-roll tests in wind tunnel. The point of this modeling method was the summation of several sine waves for which the frequencies were corresponding to a main frequency and several subfrequencies that were whole-number multiples of the main frequency, and the coefficients in the dynamic equations were all calculated from the frequency analysis.

II. Frequency Spectrum Analysis to Time History of Wing Rock

A. Frequency Structure of Free-to-Roll Time History

The experimental data for wing rock were all from [10], where the experimental model used was a wing body with a 30° sweep, as shown in Fig. 1, and for other geometric models (e.g., a delta wing with high sweep), the analysis method was similar. The experiments were performed in the D-4 wind tunnel of the Beijing University of Aeronautics and Astronautics, which was a low-turbulence, 1.5 by 1.5 m, low-speed wind tunnel. An artificial perturbation was glued onto the tip of the model, and the perturbation was a microparticle with a diameter of 0.3 mm, located at the azimuth angle of 0° around the nose [10]. Time histories of rolling angles were obtained using the free-to-roll rig with a 12-bit optical encoder, as shown in Fig. 1b. The sample rate of roll angles was 512 Hz with a resolution of 0.088°. The model did not need to be disturbed initially to start the motion and could be triggered to wing rock by the flow itself.

Figure 2a shows a roll angle time history of wing rock at a 52.5° angle of attack, and Fig. 2b shows the associated rolling angular accelerations obtained by a second-order differential operation on the roll angle time history. A finite indicial response digital filter was adopted to filter out the high-frequency noise in the time history of rolling angular accelerations, and a Hamming window was used in the process of designing the digital filter with a filter length of $N = 30$ and a cutoff frequency of 7.68 Hz. After the motion approached to a limit-cycle oscillation, as shown in Fig. 2a, fast Fourier transformation (FFT) of the filtered roll angle acceleration time history of the wing rock was conducted.

Figures 2c and 2d presented, respectively, the magnitude and phase spectrum for the frequency spectrum of the rolling angular accelerations. In Fig. 2c, some peak values of magnitude mainly appeared at the main frequency and several subfrequencies in the magnitude spectrum, which showed the frequency structure of the rolling angular accelerations. It was found that the frequencies, at which some peak values of magnitude appeared, were approximately

Received 1 December 2009; revision received 28 November 2010; accepted for publication 11 January 2011.

*Ph.D. Candidate, Ministry-of-Education Key Laboratory of Fluid Mechanics; wangbing@ase.buaa.edu.cn.

†Professor, Ministry-of-Education Key Laboratory of Fluid Mechanics; dengxueying@vip.sina.com. Senior Member AIAA.

‡Associate Professor, Ministry-of-Education Key Laboratory of Fluid Mechanics; bf-ma@buaa.edu.cn.

§Ph.D. Candidate, Ministry-of-Education Key Laboratory of Fluid Mechanics; llccdy@163.com.

¶Master Candidate, Ministry-of-Education Key Laboratory of Fluid Mechanics; cbc1985@hotmail.com.

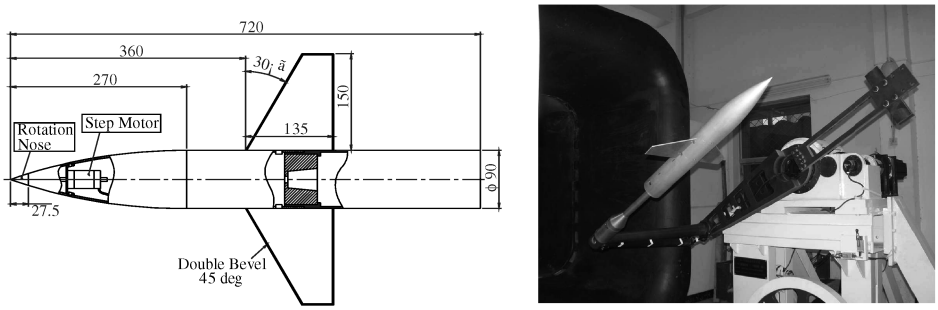

a) Model for free-to-roll tests **b) Free-to-roll apparatus**

Fig. 1 Experimental model and apparatus.

the whole number of the main frequency. The magnitude at each peak value and the associated frequency were shown in Table 1. The φ_i in Table 1 was the phase difference between the subfrequency and the main frequency, and the phase difference φ_i was translated into the range from −180 to 180°. An idea was formed that the summation of several sine waves, for which the frequencies included main frequency and several subfrequencies that were whole-number multiples of the main frequency, could shape the roll angle time history of wing rock. Based on this frequency structure and the Fourier expansion method, we could obtain the expression of the rolling angular acceleration using a Fourier series. According to the frequency analysis,

$$\phi = \sum_{i=1}^{n} A_i \sin(\omega_i t + \varphi_i) = \sum_{i=1}^{n} \phi_i \tag{1}$$

$$\dot{\phi} = \sum_{i=1}^{n} A_i \omega_i \cos(\omega_i t + \varphi_i) = \sum_{i=1}^{n} \dot{\phi}_i \tag{2}$$

$$\ddot{\phi} = -\sum_{i=1}^{n} A_i \omega_i^2 \sin(\omega_i t + \varphi_i) = \sum_{i=1}^{n} \ddot{\phi}_i \tag{3}$$

Equation (1) shows the roll angle time history using a Fourier expansion, and Eqs. (2) and (3) were the associated rolling angular rate and the rolling angular acceleration, whereA_i, w_i, and φ_i denoted the amplitude, frequency, and phase angle, respectively. The main frequency was w_1 and $w_i = iw_1$. The item of $A_i w_i^2 / A_1 w_1^2$ in Eq. (3) was equal to the magnitude at the frequency w_i in the frequency analysis, as shown in Fig. 2c and Table 1, and if A_1 was known, A_i would be obtained from this item. For simplification, in the practical superposition, only the first several sine waves were held. Then, the second-order sine waves superposition implied the summation of two sine waves for which the frequencies included main frequency and second-main frequency. It was emphasized that the second-main frequency was triple rather than double of the main frequency, because the magnitude of energy at the frequency that was triple of the main frequency was larger than the one at the frequency that was double the main frequency from the magnitude spectrum in Fig. 2c.

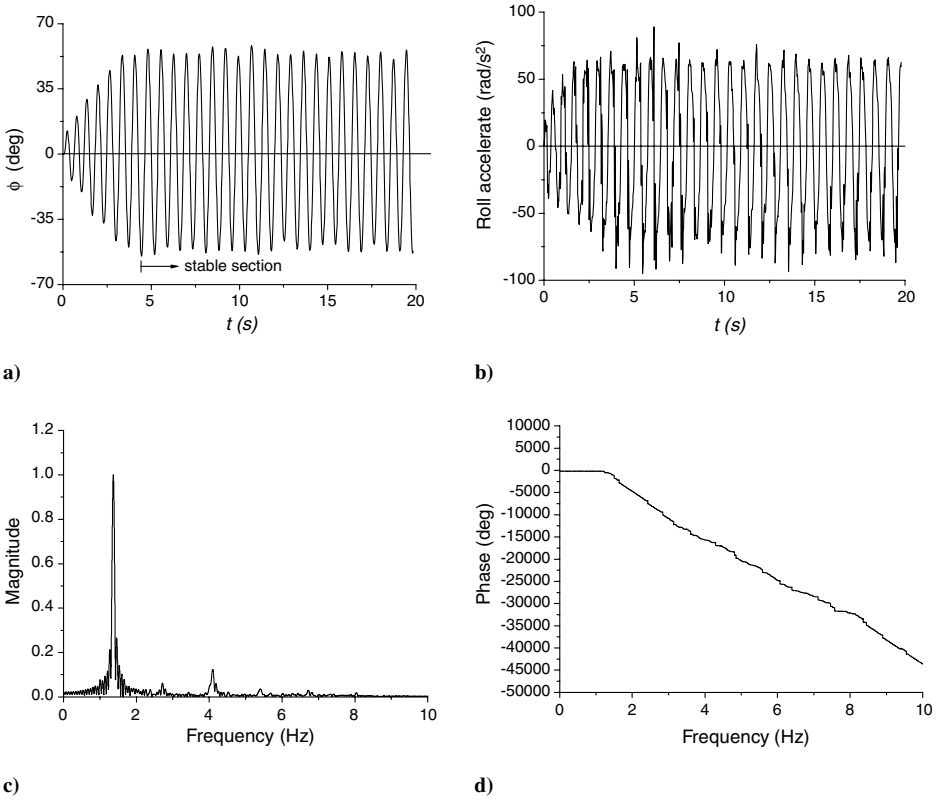

a) **b)**

c) **d)**

Fig. 2 Time history of wing rock and frequency spectrum of associated angular acceleration: a) time history of wing rock [10]; b) associated time history of rolling angular acceleration; c) associated magnitude spectrum of rolling angular accelerations; and d) associated phase spectrum of rolling angular accelerations.

Table 1 Parameters at peak values of frequency spectrum in Fig. 2

Frequency, Hz	φ_i, °	Magnitude
1.36406	0	1
2.71484	−51.86	1/16.22
4.09375	−64.64	1/8.033
5.40625	−53.27	1/28.30
6.72031	36.54	1/33.66

The third-order sine waves superposition implied the summation of three sine waves for which the frequencies included main frequency, second-main frequency and third-main frequency. The higher-order sine waves superposition obeyed the same rule.

According to Eqs. (1–3) and the preceding rule of sine waves superposition, we could shape the time history of wing rock by sine waves superposition. Figures 3a–3c show the time history for roll angles, rolling angular rate, and rolling angular acceleration using a third-order sine waves superposition, and the associated graphs for $C_l - \phi$ were shown in Figs. 4a and 4b, where

$$C_l = \frac{I_{xx}\ddot{\phi}}{(1/2)\rho u_\infty^2 Sb} \tag{4}$$

The second-order sine waves superposition shows the main characters of the $C_l - \phi$ curve of the free-to-roll data in the wind-tunnel tests, as shown in Figs. 4a and 4c. When the order of the sine waves superposition achieved more than second order, it could be seen that the curves of $C_l - \phi$ gradually converged to be one curve, as shown in Fig. 4b.

By comparing the third-order sine waves superposition with the experimental data $C_l - \phi$ in the wind tunnel, it could be seen that they were in fairly good agreement with each other, as shown in Fig. 4d. This indicated that the third-order sine waves superposition was enough to reproduce the roll angle time history and roll moment $C_l - \phi$ of wing rock.

Although it was quite different between the time history for rolling angular accelerations of the sine wave alone and that of the third-order sine superposition, as shown in Fig. 3c, there was little difference in the roll angles and roll rates time history between the sine waves alone and the third-order sine waves superposition as

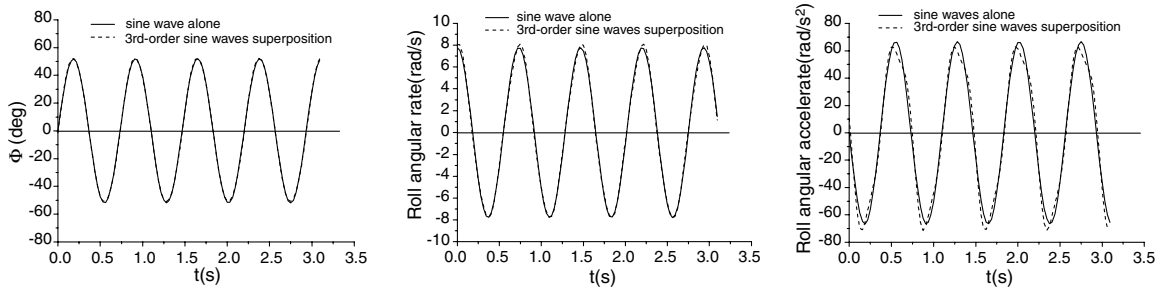

a) Roll angles **b) Rolling angular rates** **c) Rolling angular accelerations**

Fig. 3 Time history of third-order sine waves superposition.

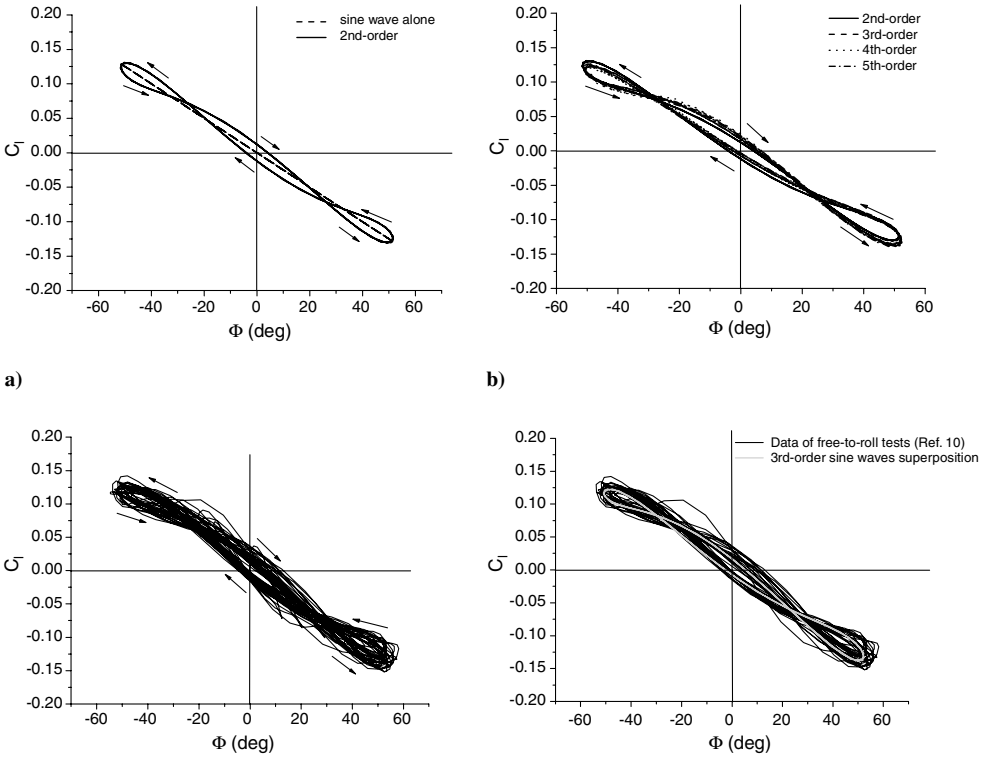

Fig. 4 a) $C_l - \phi$ of second-order sine waves superposition; b) $C_l - \phi$ of different orders of sine waves superposition; c) $C_l - \phi$ of free-to-roll experimental data in Fig. 2; and d) comparison of $C_l - \phi$ between third-order sine waves superposition and experimental data when movement approaches stable single limit-cycle oscillation.

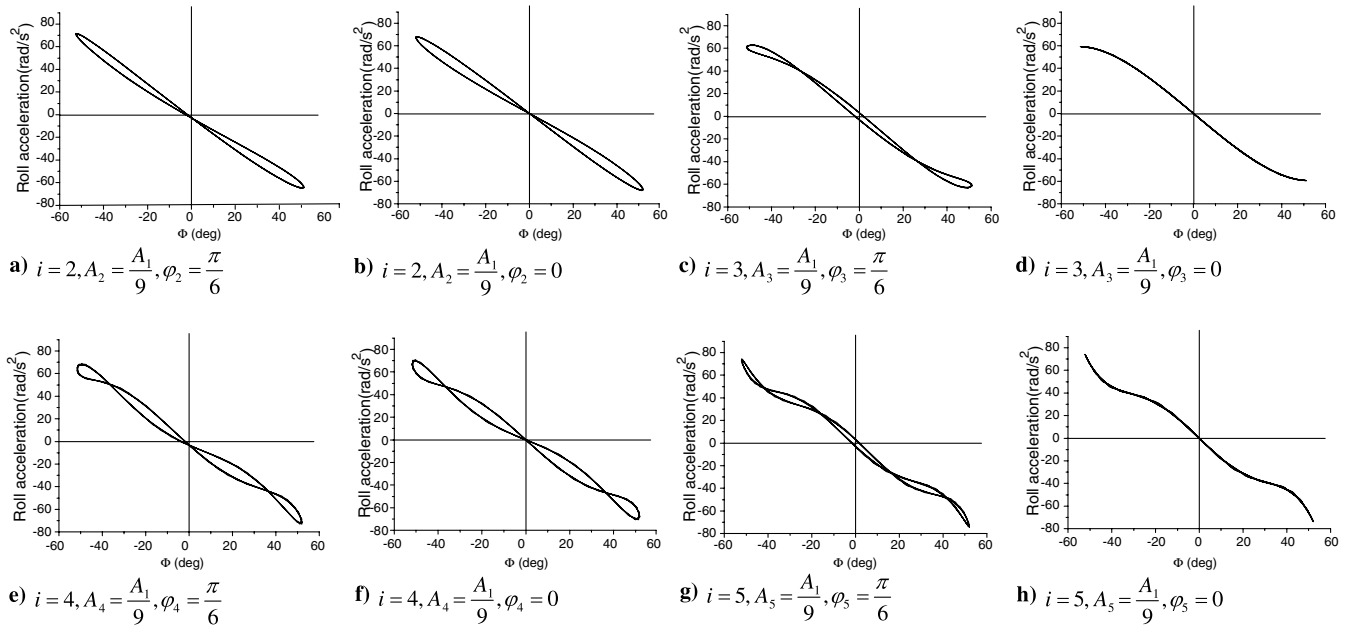

Fig. 5 Roll angular acceleration vs roll angle of two sine waves summation.

shown in Figs. 3a and 3b. Therefore, it could be obtained as approximately $\phi \approx \phi_1$ and $\dot{\phi} \approx \dot{\phi}_1$ in Eqs. (1) and (2), which was very important for modeling the wing rock in Sec. III, and it proved to be reasonable.

FFT transformations were applied on the time history of the rolling angular accelerations, rather than that of the roll angles, because the rolling angular accelerations were the second-order derivative of roll angles, as shown in Eqs. (1) and (3), and the energy magnitude of each frequency component for rolling angular accelerations was relevant to the square of the frequency. Therefore, the peak values of the energy magnitude at the higher frequencies were more obvious in the frequency spectrum for the time history of the rolling angular accelerations.

B. Analysis of Sine Functions Superposition

A two-sine summation with the frequency w_1 and the other frequency w_i ($w_i = iw_1$; $i = 2, 3, \cdots$) was studied in this section, and was expressed as follows:

$$\phi = A_1 \sin w_1 t + A_i \sin(w_i t + \varphi_i) \tag{5}$$

$$\dot{\phi} = A_1 w_1 \cos w_1 t + A_i w_i \cos(w_i t + \varphi_i) \tag{6}$$

$$\ddot{\phi} = -A_1 w_1^2 \sin w_1 t - A_i w_i^2 \sin(w_i t + \varphi_i) \tag{7}$$

In Eqs. (5–7), if φ_i was not $k\pi$ ($k = 0, 1, 2, \cdots$), the number of the closed orbits in the $\ddot{\phi} - \phi$ graph would just equal the number of i ($i = w_i/w_1$), as shown in Figs. 5a, 5c, 5e, and 5g. Then, if φ_i was $k\pi$ ($k = 0, 1, 2, \cdots$), when$i$ was an even number, the number of closed orbits in the $\ddot{\phi} - \phi$ graph would still equal the number of i, as shown in Figs. 5b and 5f, while there were no closed orbits in the graph of $\ddot{\phi} - \phi$ when i was an odd number, as shown in Figs. 5d and 5h. Therefore, it could be seen that if there were closed orbits in the graph of $C_l - \phi$, the number of the closed orbits in the graph of $C_l - \phi$ was i and $i = w_i/w_1$, in which w_1 was the main frequency and w_i was the subfrequencies.

III. Modeling of Wing Rock

A. Model Derivation

As a result (shown in Sec. II), the third-order sine waves superposition was enough to reproduce the roll angle time history of wing rock and the graph of $C_l - \phi$. Moreover, the second-order sine waves superposition showed the main characters of the $C_l - \phi$ curve of the free-to-roll data in the wind-tunnel tests. The third-order sine waves superposition was

$$\phi = \sum_{i=1}^{3} A_i \sin(w_i t + \varphi_i) \tag{8}$$

$$\dot{\phi} = \sum_{i=1}^{3} A_i w_i \cos(w_i t + \varphi_i) \tag{9}$$

$$\ddot{\phi} = -\sum_{i=1}^{3} A_i w_i^2 \sin(w_i t + \varphi_i) \tag{10}$$

and the second-order sine waves superposition was

$$\phi = A_1 \sin w_1 t + A_3 \sin(w_3 t + \varphi_3) \tag{11}$$

$$\dot{\phi} = A_1 w_1 \cos w_1 t + A_3 w_3 \cos(w_3 t + \varphi_3) \tag{12}$$

$$\ddot{\phi} = -A_1 w_1^2 \sin w_1 t - A_3 w_3^2 \sin(w_3 t + \varphi_3) \tag{13}$$

For simplification of expression, it was supposed that $w_1 = w$. So, the motion equations of the summation of three sine waves for which the frequencies included a main frequency and a double and triple of the main frequency were

$$\phi = \sum_{i=1}^{3} A_i \sin(iwt + \varphi_i) = \sum_{i=1}^{3} \phi_i \tag{14}$$

$$\dot{\phi} = \sum_{i=1}^{3} iA_i w \cos(iwt + \varphi_i) = \sum_{i=1}^{3} \dot{\phi}_i \tag{15}$$

$$\ddot{\phi} = -A_1 w^2 \sin wt - 4A_2 w^2 \sin(2wt + \varphi_2) - 9A_3 w^2 \sin(3wt + \varphi_3) \tag{16}$$

Considering $\phi \approx \phi_1$ and $\dot{\phi} \approx \dot{\phi}_1$, presented in Sec. II,

$$\frac{\ddot{\phi}}{\phi} \approx \frac{\ddot{\phi}}{\phi_1} = -w^2 - \frac{4w^2 A_2}{A_1} \frac{\sin(2wt + \varphi_2)}{\sin wt} - \frac{9w^2 A_3}{A_1} \frac{\sin(3wt + \varphi_3)}{\sin wt} \tag{17}$$

where

$$\frac{\sin(2wt+\varphi_2)}{\sin wt} = 2\cos wt\cos\varphi_2 + \frac{\cos 2wt}{\sin wt}\sin\varphi_2 \tag{18}$$

and

$$\frac{\sin(3wt+\varphi_3)}{\sin wt} = (\cos 2wt + 2\cos^2 wt)\cos\varphi_3 + \left(\frac{\cos wt\cos 2wt}{\sin wt} - 2\sin wt\cos wt\right)\sin\varphi_3 \tag{19}$$

or

$$\frac{\sin(3wt+\varphi_3)}{\sin wt} = (2\cos 2wt + 1)\cos\varphi_3 + \left(\frac{\cos wt\cos 2wt}{\sin wt} - 2\sin wt\cos wt\right)\sin\varphi_3 \tag{20}$$

The motion equations of the summation of two sine waves for which the frequencies included a main frequency and a triple of the main frequency were

$$\phi = A_1\sin wt + A_3\sin(3wt+\varphi_3) = \phi_1 + \phi_3 \tag{21}$$

$$\dot{\phi} = A_1 w\cos wt + 3A_3 w\cos(3wt+\varphi_3) = \dot{\phi}_1 + \dot{\phi}_3 \tag{22}$$

$$\ddot{\phi} = -A_1 w^2\sin wt - 9A_3 w^2\sin(3wt+\varphi_3) \tag{23}$$

Also considering $\phi \approx \phi_1$ and $\dot{\phi} \approx \dot{\phi}_1$, presented in Sec. II,

$$\frac{\ddot{\phi}}{\phi} \approx \frac{\ddot{\phi}}{\phi_1} = -w^2 - \frac{9w^2A_3}{A_1}\frac{\sin(3wt+\varphi_3)}{\sin wt} \tag{24}$$

where $[\sin(3wt+\varphi_3)]/\sin wt$ was decomposed as Eq. (19) or Eq. (20).

In the motion equations of the summation of three sine waves, presented previously, considering $\phi \approx \phi_1$ and $\dot{\phi} \approx \dot{\phi}_1$, presented in Sec. II,

$$\sin wt = \frac{\phi}{A_1}, \qquad \cos wt = \frac{\dot{\phi}}{wA_1} \tag{25}$$

And there were three different decomposition forms for $\cos 2wt$:

I)

$$\cos 2wt = 2\cos^2 wt - 1 = 2\left(\frac{\dot{\phi}}{wA_1}\right)^2 - 1 \tag{26}$$

II)

$$\cos 2wt = 1 - 2\sin^2 wt = 1 - 2\left(\frac{\phi}{A_1}\right)^2 \tag{27}$$

III)

$$\cos 2wt = \cos^2 wt - \sin^2 wt = \left(\frac{\dot{\phi}}{wA_1}\right)^2 - \left(\frac{\phi}{A_1}\right)^2 \tag{28}$$

By the use of the three preceding equations, there were four different forms of dynamic equations corresponding to the second-order sine waves superposition. For the third-order sine waves superposition, there would be 12 forms of dynamic equations.

According the method of the sine waves superposition, the second-order sine waves superposition could reproduce the main character of a free-to-roll motion, as shown in Figs. 4a and 4c. To simplify the process to obtain the right dynamic equation corresponding to the third-order sine waves superposition, the classification of the four dynamic equations corresponding to the preceding second-order sine waves superposition was conducted first.

Substituting the three different decomposition forms of $\cos 2wt$ into the motion equations corresponding to the second-order sine waves superposition, the motion equations could be obtained as follows:

I)

$$\ddot{\phi} = -w^2\left(1 - \frac{9A_3}{A_1}\cos\varphi_3\right)\phi + \frac{9wA_3\sin\varphi_3}{A_1}\dot{\phi} + \frac{18wA_3\sin\varphi_3}{A_1^3}\phi^2\dot{\phi} - \frac{36A_3\cos\varphi_3}{A_1^3}\phi\dot{\phi}^2 - \frac{18A_3\sin\varphi_3}{wA_1^3}\dot{\phi}^3 \tag{29}$$

II)

$$\ddot{\phi} = -w^2\left(1 + \frac{9A_3}{A_1}\cos\varphi_3\right)\phi + \frac{18w^2A_3\cos\varphi_3}{A_1^3}\phi^3 + \frac{9wA_3\sin\varphi_3}{A_1^3}\phi^2\dot{\phi} - \frac{18A_3\cos\varphi_3}{A_1^3}\phi\dot{\phi}^2 - \frac{9A_3\sin\varphi_3}{wA_1^3}\dot{\phi}^3 \tag{30}$$

III)

$$\ddot{\phi} = -w^2\left(1 + \frac{27A_3}{A_1}\cos\varphi_3\right)\phi + \frac{36w^2A_3\cos\varphi_3}{A_1^3}\phi^3 - \frac{9wA_3\sin\varphi_3}{A_1}\dot{\phi} + \frac{36wA_3\sin\varphi_3}{A_1^3}\phi^2\dot{\phi} \tag{31}$$

IV)

$$\ddot{\phi} = -w^2\phi + \frac{9w^2A_3\cos\varphi_3}{A_1^3}\phi^3 + \frac{9wA_3\sin\varphi_3}{A_1^3}\phi^2\dot{\phi} - \frac{27A_3\cos\varphi_3}{A_1^3}\phi\dot{\phi}^2 - \frac{9A_3\sin\varphi_3}{wA_1^3}\dot{\phi}^3 \tag{32}$$

To classify these four dynamic equations corresponding to the second-order sine waves superposition, the analysis to them was conducted.

From the frequency spectrum of rolling angular accelerations in Fig. 2c and Table 1 in Sec. II, it could be obtained that $\varphi_2 = -51.86°$, $\varphi_3 = -64.64°$, $A_2 = A_1/(4\times 16.22)$, $A_3 = A_1(9\times 8.033)$, $f =$ 1.364 Hz, and $w = 2\pi f$ in Eqs. (29–32). Because there was little difference between the roll angle time history of the sine wave alone, for which the frequency was the main frequency, and that of the third-order sine waves superposition, as shown in Fig. 3a, A_1 was approximately equal to the average amplitude of the free-to-roll oscillation, which was 52°.

To write Eqs. (29–32) each as first-order systems, we let $x = \phi$, $y = \dot{\phi}$, and these four equations correspond to four first-order systems. As a result, the critical points of the equivalent first-order system corresponding to Eqs. (29–32) were determined, and the types of determined critical points and system stability were analyzed by the use of the parameters determined previously.

Among these equivalent first-order systems, only the system corresponding to Eq. (31) has a close trajectory in the phase plane portrait. This was the period solution of a limit-cycle oscillation, which was the one we just tried to find to model the limit cycle of wing rock.

According to the roll angle time history of free-to-roll experiments, the phase plane trajectories would approach to a limit cycle. From the analysis of Eqs. (29–32), only Eq. (31) satisfied this character. That is,

$$\ddot{\phi} = -w^2\left(1 + \frac{27A_3}{A_1}\cos\varphi_3\right)\phi + \frac{36w^2A_3\cos\varphi_3}{A_1^3}\phi^3 - \frac{9wA_3\sin\varphi_3}{A_1}\dot{\phi} + \frac{36wA_3\sin\varphi_3}{A_1^3}\phi^2\dot{\phi}$$

As a result, that part of the sine waves superposition, including the main frequencies and the subfrequency, which was triple the main frequency, should be modeled like the preceding form.

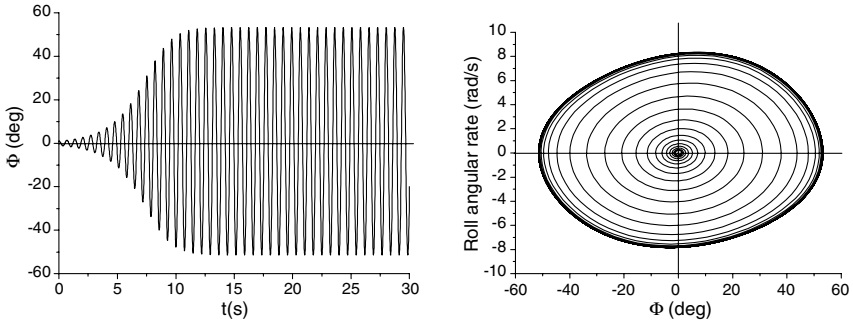

a) b)

Fig. 6 a) time history of roll angles of the numerical simulation by the modeling dynamics equation, and b) phase plane portrait, with initial conditions $\phi(0) = 1°$ and $\dot{\phi}(0) = 0$.

So, when substituting the three different decomposition forms of $\cos 2wt$ into the third-order motion equations, there were three forms of dynamic equations corresponding to the third-order sine superposition remaining. They were as follows:

I)

$$\ddot{\phi} = -w^2\left(1 + \frac{27A_3}{A_1}\cos\varphi_3\right)\phi + \frac{36w^2A_3\cos\varphi_3}{A_1^3}\phi^3 - \frac{9wA_3\sin\varphi_3}{A_1}\dot{\phi} - \frac{8wA_2\cos\varphi_2}{A_1^2}\phi\dot{\phi} + \frac{36wA_3\sin\varphi_3}{A_1^3}\phi^2\dot{\phi} - \frac{8A_2\sin\varphi_2}{A_1^2}\dot{\phi}^2 + 4w^2A_2\sin\varphi_2 \tag{33}$$

II)

$$\ddot{\phi} = -w^2\left(1 + \frac{27A_3}{A_1}\cos\varphi_3\right)\phi + \frac{8w^2A_2\sin\varphi_2}{A_1^2}\phi^2 + \frac{36w^2A_3\cos\varphi_3}{A_1^3}\phi^3 - \frac{9wA_3\sin\varphi_3}{A_1}\dot{\phi} - \frac{8wA_2\cos\varphi_2}{A_1^2}\phi\dot{\phi} + \frac{36wA_3\sin\varphi_3}{A_1^3}\phi^2\dot{\phi} - 4w^2A_2\sin\varphi_2 \tag{34}$$

III)

$$\ddot{\phi} = -w^2\left(1 + \frac{27A_3}{A_1}\cos\varphi_3\right)\phi + \frac{4w^2A_2\sin\varphi_2}{A_1^2}\phi^2 + \frac{36w^2A_3\cos\varphi_3}{A_1^3}\phi^3 - \frac{9wA_3\sin\varphi_3}{A_1}\dot{\phi} - \frac{8wA_2\cos\varphi_2}{A_1^2}\phi\dot{\phi} + \frac{36wA_3\sin\varphi_3}{A_1^3}\phi^2\dot{\phi} - \frac{4A_2\sin\varphi_2}{A_1^2}\dot{\phi}^2 \tag{35}$$

To determine which equation would be most reasonable to model the limit-cycle oscillation of wing rock in Fig. 2, the analysis of Eqs. (33–35) was conducted as that of the dynamic equations corresponding to the preceding second-order sine waves superposition, and we let $x = \phi$ and $y = \dot{\phi}$.

Although for the three equivalent first-order systems corresponding to Eqs. (33–35) there was a limit-cycle solution existing in the phase portrait of each, the equilibrium positions of the limit cycles were (−2.1745°, 0), (2.1669°, 0) and (0, 0), respectively. According to the roll angle time history of wing rock in the wind-tunnel tests, as shown in Fig. 2, the equilibrium position of the limit-cycle oscillations was (0, 0), so Eq. (35) was the only one to own this nature. As a result, Eq. (35) was the most reasonable dynamic equation to model the limit-cycle oscillation of wing rock. That is,

$$\ddot{\phi} = -w^2\left(1 + \frac{27A_3}{A_1}\cos\varphi_3\right)\phi + \frac{4w^2A_2\sin\varphi_2}{A_1^2}\phi^2 + \frac{36w^2A_3\cos\varphi_3}{A_1^3}\phi^3 - \frac{9wA_3\sin\varphi_3}{A_1}\dot{\phi} - \frac{8wA_2\cos\varphi_2}{A_1^2}\phi\dot{\phi} + \frac{36wA_3\sin\varphi_3}{A_1^3}\phi^2\dot{\phi} - \frac{4A_2\sin\varphi_2}{A_1^2}\dot{\phi}^2$$

B. Simulation of Wing Rock

Equation (35) is used to model a limit-cycle oscillation of wing rock, and the numerical solution of this modeling dynamic equation is shown in Fig. 6. By comparing the solution of $C_l - \phi$ from the modeled dynamic equation with that from the corresponding sine waves superposition, it can be seen they were in fairly good agreement with each other, as shown in Figs. 7a and 7b. These results indicated that it was reasonable to suppose that $\phi \approx \phi_1$ and $\dot{\phi} \approx \dot{\phi}_1$ in the process of modeling the wing rock previously. Figure 7c shows the comparison results between the solution of the dynamic equation (35) and the experimental data; they agreed fairly well with each other. This indicated that modeling dynamic equation corresponding to the third-order sine waves superposition could model the limit-cycle oscillation of wing rock, as shown in Fig. 2.

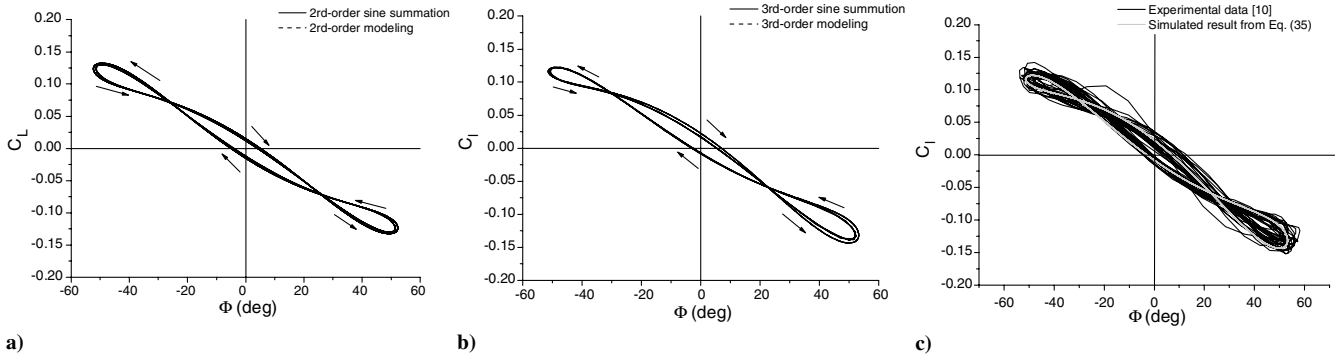

a) b) c)

Fig. 7 Comparison of $C_l - \phi$ for sine superposition and corresponding dynamic simulations: a) second-order results, b) third-order results, and c) third-order simulation and experimental data.

IV. Conclusions

A novel method for modeling wing rock of one degree of freedom was presented based on the frequency spectrum analysis to the wind-tunnel free-to-roll tests data of wing rock. From the frequency analysis of the time history of rolling angular accelerations of the wing rock, it was found that there were other higher-frequency components, except the main frequency, and the energy at the triple-main frequency among them was greater than others. The central idea of the method presented for modeling wing rock was the summation of several sine waves for which the frequencies included main frequency, double-main frequency, and triple-main frequency. The coefficients of the modeling dynamic equations were all determined by the frequency analysis of the time history of rolling angular accelerations of the wing rock. The solution of the modeling dynamic equation was in fairly good agreement with the experimental data. It indicated that the modeling dynamic equation corresponding to the third-order sine waves superposition could model the limit-cycle oscillation of wing rock.

Acknowledgment

This work is supported by the National Natural Science Foundation of China under grant nos. 10702004 and 10872019.

References

[1] Katz, J., "Wing/Vortex Interactions and Wing Rock," *Progress in Aerospace Sciences*, Vol. 35, No. 7, 1999, pp. 727–750. doi:10.1016/S0376-0421(99)00004-4

[2] Nelson, R. C., and Pelletier, A., "The Unsteady Aerodynamics of Slender Wings and Aircraft Undergoing Large Amplitude Maneuvers," *Progress in Aerospace Sciences*, Vol. 39, Nos. 2–3, 2003, pp. 185–248. doi:10.1016/S0376-0421(02)00088-X

[3] Nguyen, L. T., Yip, L. P., and Chambers, J. R., "Self-Induced Wing Rock of Slender Delta Wings," AIAA Paper 1981-1883, Aug. 1981.

[4] Hsu, C. H., and Lan, C. E., "Theory of Wing Rock," *Journal of Aircraft*, Vol. 22, No. 10, Oct. 1985, pp. 920–924. doi:10.2514/3.45225

[5] Konstadinopoulos, P., Mook, D. T., and Nayfeh, A. H., "Subsonic Wing Rock of Slender Delta Wings," *Journal of Aircraft*, Vol. 22, No. 3, Aug. 1985, pp. 223–228. doi:10.2514/3.45111

[6] Elzebda, J. M., Nayfeh, A. H., and Mook, D. T., "Development of an Analytical Model of Wing Rock for Slender Delta Wings," *Journal of Aircraft*, Vol. 26, No. 8, Aug. 1989, pp. 737–743. doi:10.2514/3.45833

[7] Nayfeh, A. H., Elzebda, J. M., and Mook, D. T., "Analytical Study of the Subsonic Wing-Rock Phenomenon for Slender Delta Wings," *Journal of Aircraft*, Vol. 26, No. 9, Aug. 1989, pp. 805–809. doi:10.2514/3.45844

[8] Guglieri, G., and Quagliotti, F., "Experimental Observation and Discussion of the Wing Rock Phenomenon," *Aerospace Science and Technology*, Vol. 1, No. 2, 1997, pp. 111–123. doi:10.1016/S1270-9638(97)90041-9

[9] Yang, G. W., Lu, X. Y., Zhuang, L. X., Weishäupl, C., and Laschka, B., "Nonlinear Analysis of Dynamics Stability and the Prediction of Wing Rock," *Journal of Aircraft*, Vol. 39, No. 1, Jan–Feb. 2002, pp. 84–90. doi:10.2514/2.2899

[10] Ma, B. F., "Experimental Investigation of Roll Oscillation Induced by Forebody Vortex," Postdoctoral Research Rept., Beijing Univ. of Aeronautics and Astronautics, PRC, July 2007 (in Chinese).